

# A Novel Rotating-Wave X-Ray Source for Analysis of the Martian Landscape

Jose E. Velazco,\* Mark Taylor,\* Yang Liu,† Robert Hodyss,† and Abby Allwood†

**ABSTRACT.** — In this article, we present analysis and computer simulations for a new accelerator concept that we are proposing for exploration of various planetary surfaces, including the Martian landscape. The rotating-wave accelerator (RWA) uses rotating-wave fields and an external magnetic field to produce acceleration of a low-energy electron beam to high velocities. X-rays are produced by the electrons upon impinging on a suitable target. A linear analysis of the accelerating process is presented as well as computer simulations. These studies show that the RWA can successfully achieve 200-keV X-rays; energy that is ideally suited for X-ray analysis on Mars and other planetary missions. The RWA development will enable a new generation of very compact, power-efficient imaging and analytical instruments capable of producing high-energy X-rays for standoff planetary surface X-ray analysis such as fluorescence and tomography.

## I. Introduction

JPL's Communications Ground Systems Section (333) is employing its expertise in transmitters and vacuum tube design, commonly used for the Deep Space Network, in the development of advanced X-ray sources for the exploration of the Martian landscape and other planetary surfaces. Section 333 and the Planetary Science Section (322) are collaborating in the development of a new X-ray source that we refer to as the rotating-wave X-ray source (RWXS). The RWXS should be able to produce X-rays in the 100- to 200-keV energy range in a very compact structure. X-ray analysis has been used or proposed in Mars surface missions (Alpha Particle X-Ray Spectrometer, or APXS [1]; Chemistry and Mineralogy X-Ray Diffraction instrument, or CheMin; [2]; Planetary Instrument for X-Ray Lithochemistry, or PIXL [3]) with either a radionuclide source or an X-ray tube capable of 28-keV energy. A high X-ray energy source (such as the RWXS) with an operating voltage similar to or lower than 28 kV would enable a new generation of X-ray analysis science instruments for Martian and other planetary surface and orbital missions. The advantages of a high X-ray energy and high-flux RWXS source include X-ray analysis (e.g., fluorescence or tomography) with better depth penetration and the ability to excite the strong K lines of the entire

---

\* Communications Ground Systems Section.

† Planetary Science Section.

The research described in this publication was carried out by the Jet Propulsion Laboratory, California Institute of Technology, under a contract with the National Aeronautics and Space Administration. © 2016 California Institute of Technology. U.S. Government sponsorship acknowledged.

element periodic table. Such a source allows for standoff material composition analysis from several meters. An additional revolutionary RWXS feature is that it will also be able to penetrate the targets and provide information at various target depths using a combination of X-ray spectroscopy and backscatter imaging.

The RWXS (Figure 1) will incorporate a novel rotating-wave accelerator (RWA) [4–6] that uses rotating waves (circularly polarized fields) to efficiently accelerate a low-energy electron beam to high energies in a very short structure. The purpose of the RWA is to accelerate electrons from low energies (low velocity) to higher velocities that approach the speed of light. In similar fashion to high-power klystron amplifiers, the RWA consists of a microwave cavity, an electron beam, and a set of magnetic coils to focus the beam. However, unlike klystrons where the cavity fields decelerate the electron beam, the RWA uses the cavity fields to accelerate the electrons. The resulting electron beam approaches the speed of light and is well suited for the production of high-energy X-rays.

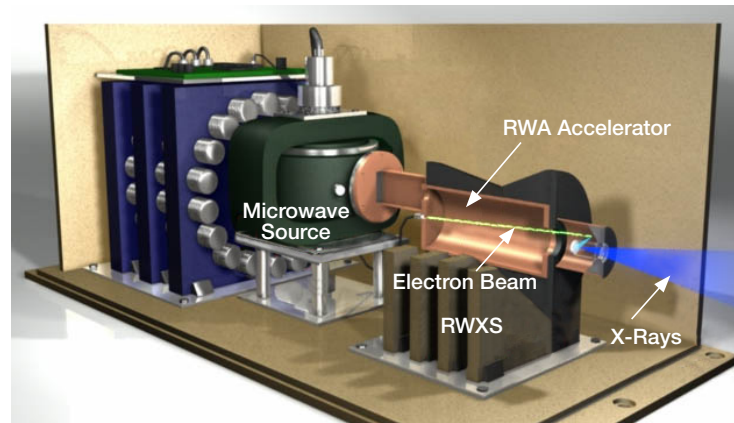


**Figure 1. Illustration of the RWXS instrument showing the cylindrical accelerating cavity, magnets, and electron beam.**

In this article, we provide a simple linear theory of the RWA acceleration process. Subsequently, we present calculations that show the amount of power necessary to operate the RWXS. We conclude with presenting computer simulations obtained using High-Frequency Structure Simulator (HFSS)<sup>1</sup> and MAGIC<sup>2</sup> to optimize the beam acceleration process for the RWXS we are proposing for X-ray analysis of planetary landscapes.

## **II. RF Accelerator Cavity Resonator**

Intensive studies of synchronous beam-wave interactions have been carried out by the authors of this article in related works<sup>3</sup> [7–11]. In the mechanism proposed herein, beam acceleration is obtained in a transverse-magnetic ( $TM_{110}$ ) rotating-mode cylindrical resona-

---

<sup>1</sup> *High-Frequency Structure Simulator's User's Manual*, ANSYS, Canonsburg, Pennsylvania.

<sup>2</sup> *MAGIC User's Manual*, Orbital ATK, Inc., Newington, Virginia.

<sup>3</sup> J. E. Velazco, "The Study of Synchronous Beam-Wave Interactions for the Generation of Coherent Microwave Radiation," PhD Dissertation, George Mason University, 1994.

tor along with an axisymmetric magnetostatic focusing field. To produce continuous beam acceleration, the static magnetic field along this cavity is adjusted to force the electrons' gyrofrequency to be equal to the drive frequency. Under this gyro-resonant condition, the beam electrons will undergo acceleration, maintaining strong temporal coherence with the radio frequency (RF) rotating mode. These dynamics are similar to the beam dynamics in a transverse-electric (TE<sub>111</sub>) mode accelerator-resonator [12] with the difference that here the beam is deflected by a transverse rotating RF magnetic field and accelerated by an axial electrical field. The intensity of the RF field inside the cavity is adjusted so that the beam is coherently accelerated to the required beam energy level. Next we present a linear analysis of the beam dynamics along the RF accelerator.

We shall assume an ideally small-diameter beam moving along an axisymmetric static magnetic field  $B = \hat{z}B_o$  with a velocity  $\nu = \hat{x}\nu_x + \hat{y}\nu_y + \hat{z}\nu_z$ . The motion of the beam-centroid inside a TM<sub>110</sub> rotating mode cavity is governed by the general equation

$$\frac{d}{dt}(m\gamma v) = -|e| \left[ \tilde{E} + v \times \tilde{B} - B_o v \times \hat{z} \right] \quad (1)$$

where  $\tilde{E}$  and  $\tilde{B}$  are, respectively, the RF electric and magnetic fields present,  $B_o$  is the amplitude of the static magnetic field, and  $\gamma$  is the electron's energy normalized to its rest energy. For a TM<sub>110</sub> rotating mode resonator, the complete set of equations, in cylindrical coordinates  $(r, \phi, z)$ , is given by [10]

$$\tilde{B}(r, \phi, z; t) = \hat{\phi} 2B_{rf} J_1(k_{\perp} r) \sin(\omega t - \phi) + \hat{r} 2B_{rf} \frac{1}{k_{\phi} r} J'_1(k_{\perp} r) \cos(\omega t - \phi) \quad (2)$$

$$\tilde{E}(r, \phi, z; t) = \hat{z} 2B_{rf} J_1(k_{\perp} r) \sin(\omega t - \phi) \quad (3)$$

where  $B_{rf}$  is a constant that describes the RF magnetic field amplitude near-axis,  $J_1$  is the first-order Bessel function of the first kind,  $k_{\perp} = u_{11}/a$  is the radial wavenumber,  $u_{11}$  is the first root of  $J_1(u_{11}) = 0$ ,  $J'_1 = \frac{d}{dk_{\perp} r} [J_1(k_{\perp} r)]$ ,  $a$  is the cavity radius, and  $\omega$  is the drive radian frequency, which for this mode is defined as

$$\omega = ck_{\perp} = \frac{u_{11}c}{a}. \quad (4)$$

The above field equations present no axial coordinate dependence and thus are the same at any  $z$ -plane within the cavity. Also, inspection of the phase argument of these fields allows the easy derivation of the azimuthal velocity of the fields,  $\Omega_{rot} \equiv d\phi/dt = \omega$  [10,13]. Consequently, in this mode the fields resonate and rotate azimuthally at  $\omega$ , i.e., they perform one gyration about the cavity axis in one RF period. The field lines for the electric and magnetic fields of this mode are shown in Figure 2.

The beam-wave interaction occurs near axis where the argument  $k_{\perp} r \ll 1$ . The field equations in the paraxial region, in rectangular coordinates  $(x, y, z)$ , are

$$\tilde{E}(x, y, t) = \frac{B_{rf}}{\omega} \left[ x \cos(\omega t) + y \sin(\omega t) \right] \hat{z} \quad (5)$$

$$\tilde{B}(x, y, t) = B_{rf} \left[ \hat{x} \cos(\omega t) + \hat{y} \sin(\omega t) \right]. \quad (6)$$

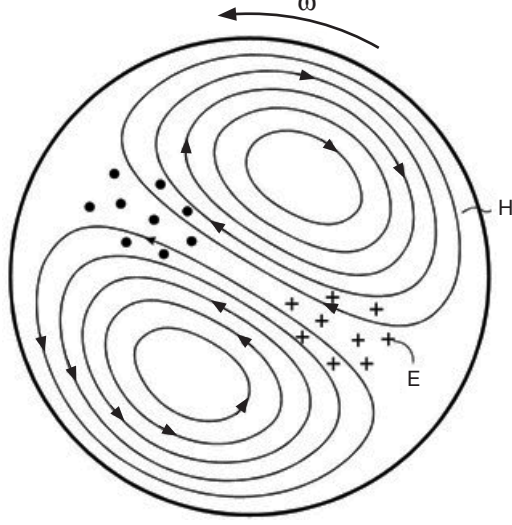


Figure 2. Field lines of electric and magnetic fields in  $TM_{110}$  rotating mode.

This rotating mode presents a constant magnetic field on-axis, and an electric field that approaches zero on-axis but that, off-axis, grows linearly with the values of the  $x$ - $y$  coordinates.

Next, we calculate the equations of motion of the electron beam as it moves inside the cavity under the influence of the rotating-mode  $TM_{110}$  fields and the static magnetic field.

To solve the general equation of motion of the beam-centroid, we assume that the fields inside the cavity are small. This allows us to consider the axial velocity and relativistic mass factor to be a constant. The beam is injected into the cavity at  $t = t_o$  and exits the cavity at  $t = t_o + \tau$ , where  $\tau$  is the electron's transit time along the cavity. Defining the transverse velocity and transverse displacement of the beam as  $\nu_{\perp} \equiv \nu_x + i\nu_y$  and  $\zeta_{\perp} \equiv x + iy$ , respectively, the solution of Equation (1) for a beam entering the cavity at the injection time  $t_o$  yields the following equations of motion:

$$\nu_{\perp}(x, y, t) = \frac{-\nu_z \Omega_{rf}}{[\Omega_c - \omega]} \exp(i\omega t) \left\{ \exp[i(\Omega_c - \omega)\tau] - 1 \right\} \quad (7)$$

$$\zeta_{\perp}(x, y, t) = -i \frac{\nu_z}{\omega} \frac{\Omega_{rf}}{(\Omega_c - \omega)} \exp(i\omega t_o) \times \left[ \exp[i\omega\tau] \left\{ \frac{\omega}{\Omega_c} \exp[i(\Omega_c - \omega)\tau] - 1 \right\} - \frac{\omega}{\Omega_c} + 1 \right] \quad (8)$$

where  $\Omega_c = eB_o/m_o\gamma_o$  is the relativistic gyrofrequency of the electrons,  $\Omega_{rf} = eB_{rf}/m_o\gamma_o$ ,  $\nu_z$  is the beam parallel velocity, here assumed constant, and  $\gamma_o$  is the relativistic factor at  $t = t_o$ .

To calculate the change in beam energy  $\gamma mc^2$  as it traverses the cavity, under different values of magnetic field ( $\Omega_c$ ), we shall use the unperturbed electron orbits given by Equation (8). For a single particle moving with a constant velocity,  $\nu_z$ , the rate of change in the particle's energy can be calculated as follows:

$$\frac{d}{dt}(\gamma mc^2) = -|e| \nu_z E_z. \quad (9)$$

The value of the electrons' energy  $\gamma(t)$  at any time  $t$  during this interaction has been calculated by replacing Equations (5) and (8) in Equation (9) and solving as

$$\gamma(t) = \gamma_o \left[ 1 - \beta_z^2 \left( \frac{\Omega_{rf}}{\Omega_c} \right)^2 \times F \left( \frac{\Omega_c}{\omega} \right) \right] \quad (10)$$

where  $\beta_z = \nu_z/c$  and  $F(\Omega_c/\omega)$  is a frequency factor defined as

$$F \left( \frac{\Omega_c}{\omega} \right) = \frac{\Omega_c}{\omega} \times \frac{1}{\left( \frac{\Omega_c}{\omega} - 1 \right)} \times \left[ \frac{1}{\left( \frac{\Omega_c}{\omega} - 1 \right)} \times \left\{ \cos [(\Omega_c - \omega)\tau] - 1 \right\} + \left( 1 - \frac{\Omega_c}{\omega} \right) \times [\cos \omega\tau - 1] \right]. \quad (11)$$

Figure 3 illustrates the frequency factor as a function of interaction time of the beam in the “scanner” resonator for different conditions of  $\frac{\Omega_c}{\omega}$ . It can be observed that under the gyroresonant condition  $\Omega_c = \omega$ , the beam gradually extracts energy from the RF fields of the input resonator and consequently undergoes acceleration as it is coherently spun up by the rotating RF fields.

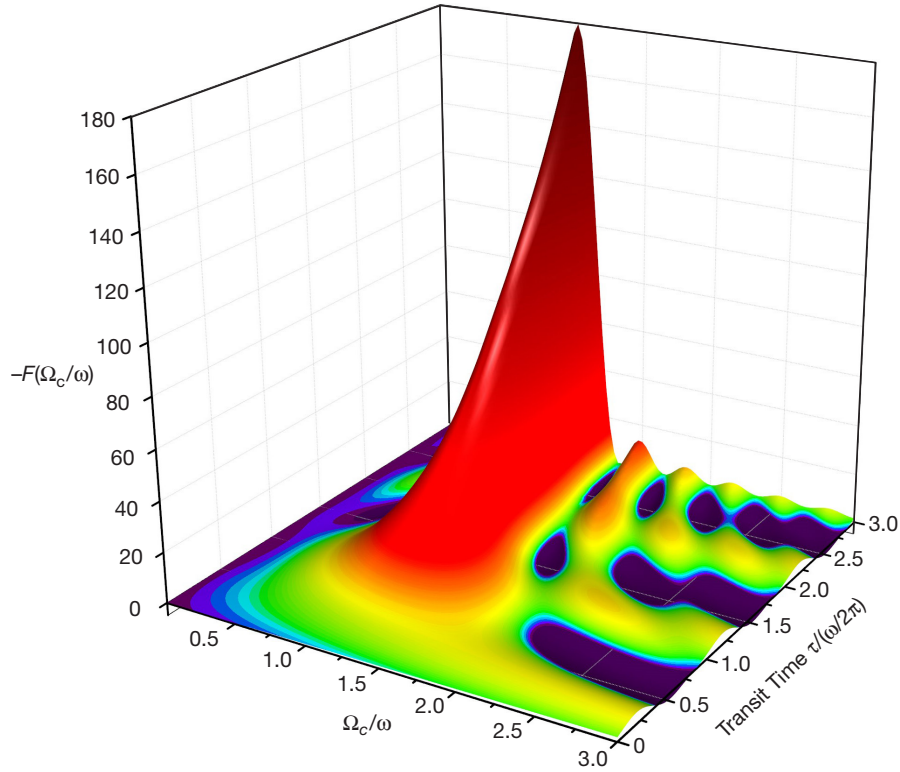


Figure 3. Plot of frequency factor,  $F$ , as a function of interaction time  $\tau$  and  $\Omega_c/\omega$  ratio.

### III. Input RF Power

We have also calculated the amount of microwave power necessary to produce beam acceleration. For a cylindrical cavity of radius  $a$  and length  $L$ , working at a frequency  $\omega$ , the input power is given as

$$P_i = (P_L + P_b) \cdot DC \quad (12)$$

where  $DC$  is the duty cycle,  $P_L$  is the power lost to the cavity walls defined as

$$P_L = \frac{R_s \pi}{Z_o^2} [caJ_o(k_{\perp} a)]^2 B_{rf}^2 \left( \frac{L}{a} + 1 \right), \quad (13)$$

and  $P_b$  is the amount of power absorbed by the beam, given by

$$P_b = I_o V_f \quad (14)$$

where  $R_s$  is the resistivity of the cavity walls in ohms,  $Z_o = 377$  ohms is the intrinsic impedance of free space,  $V_f$  is the final energy of the beam, and  $I_o$  is the beam current. For example, in order to accelerate a 3-kV, 1-mA beam to a final energy of 200 keV (at 1 mA), the required average input power for an 8-GHz copper cavity operating with a duty cycle of 0.001 (0.1 percent) would be 0.8 W. From the required 0.8 W, the cavity walls will dissipate most of the required power (0.7 W), whereas 0.1 W will be added to the beam.

### IV. Computer Simulations

During this effort, we conducted a series of computer simulations of the RWA in order to optimize electron acceleration to 200 keV. The computer simulations were conducted first by generating an HFSS RF model, and thereafter coded with MAGIC. We followed the following steps during this work:

- We first selected the cavity diameter and length suitable for operation at 8 GHz.
- Next, we used HFSS to optimize the cavity dimensions so as to achieve successful operation at 8 GHz in the  $TM_{110}$  mode.
- We then input the HFSS-optimized dimensions into MAGIC and performed time-dependent beam interaction simulations to observe the interactions between the electrons and  $TM_{110}$  circularly polarized fields.
- We subsequently optimized the RF electric field inside the cavity and focusing magnetic field with the goal of accelerating the electron beam to 200 keV.

A general picture of the RWXS is shown in Figure 1, where one can see the electron beam, accelerating cavity, X-ray target, and focusing magnet. In the RWA, an electron beam, generated by the electron gun, is injected into the accelerating cavity. Electrons moving along the cavity interact with the microwave fields and focusing field produced by the external magnet. The intensity of the microwave and focusing fields was optimized so as to provide continuous acceleration of the electrons. Upon exiting the cavity, the accelerated electrons impinge on a suitable X-ray target to produce high-energy X-rays. Key features of the RWA

accelerator are its compactness and power efficiency, making it ideal as an X-ray source for the current RWXS application.

The RWA cavity, shown in Figure 4, is cylindrical in geometry and has a radius  $a$  and length  $L$ . The cavity radius  $a$  is related to the frequency of operation by the relationship given by Equation (4). For the current application, we are considering a frequency of operation of 8 GHz, which yields a cavity radius  $a = 0.9$  in. The cavity length  $L$  is adjusted for optimum acceleration. A drawing of the resulting RWA cavity is shown in Figure 5.

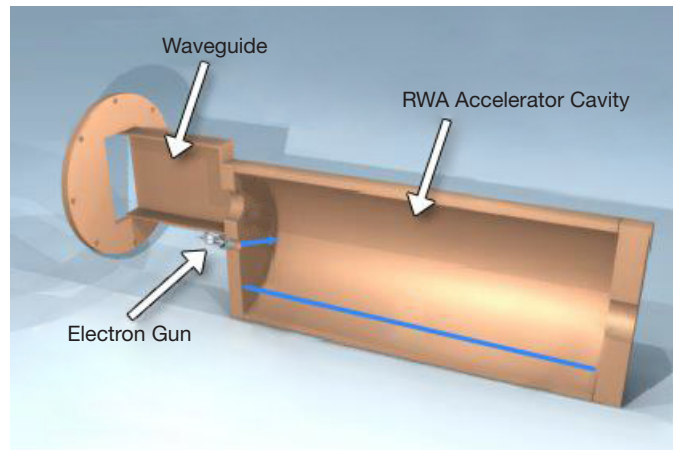


**Figure 4. Schematic of cylindrical RWA accelerator cavity showing internal dimensions.**

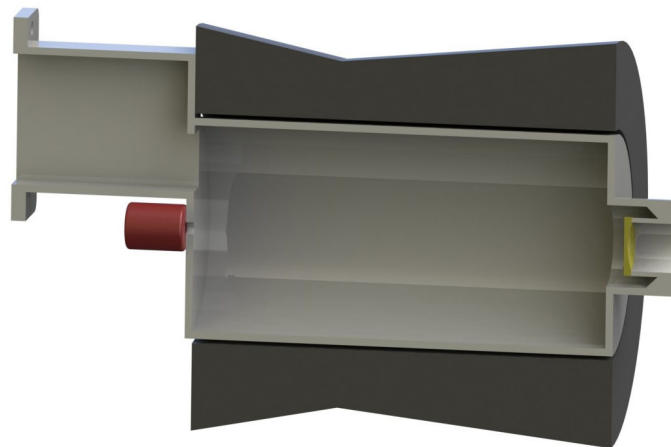


**Figure 5. SolidWorks mechanical drawing of the RWA cavity.**

After having selected the RWA cavity dimensions, we input the cavity geometry into the electromagnetic simulator HFSS in order to verify that the cavity operates in the  $TM_{110}$  mode for the desired frequency. We ran a large number of simulations in HFSS to fine-tune the tunnel at the right end of the cavity (see Figure 5) to simultaneously allow for the free passage of the accelerated electrons while minimizing field distortions. A beam tunnel with appropriate values of diameter and length was selected. In addition, we added a rectangular waveguide to the front end of the cavity for injection of the microwaves into the RWA. The resulting HFSS cavity model is shown in Figure 6.

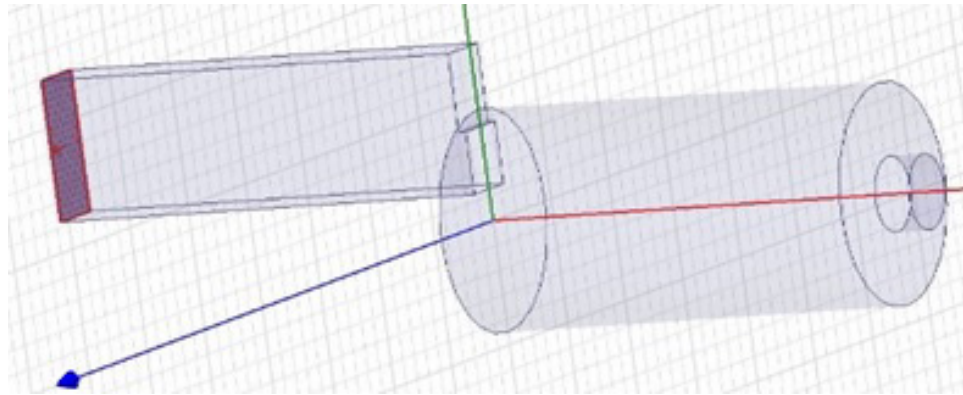


**Figure 6. HFSS model of the RWA cavity including coupling rectangular waveguide and beam tunnel.**

In Figure 7, we show a typical successful HFSS simulation result of the RWA cavity modeling at 8 GHz. Inside the rectangular waveguide, an 8-GHz wave is launched that generates a  $TE_{10}$  mode within the waveguide. This wave is coupled into the RWA resonator via a coupling iris, which, in turn, generates the required  $TM_{110}$  mode inside the cavity. The mode pattern can be clearly seen, represented by two peaks (in red), which confirm the  $TM_{110}$  mode. Once we obtained successful HFSS results with the selected cavity geometry, we moved on to perform computer simulations in MAGIC.

The code MAGIC is a particle-in-cell time-dependent plasma physics code that allows the self-consistent interaction modeling of electromagnetic fields and charged particles. We entered the RWA geometry into MAGIC (cavity radius  $a = 0.9$  in. and the appropriate cavity length  $L$ ) and also generated an electron beam along the axis of the device. Furthermore, we added an external focusing magnetic field, which is required for successful acceleration of the electrons. We then adjusted the magnetic field and RF fields inside the cavity in order to optimize electron acceleration. In Figure 8, we show a complete MAGIC simulation result of the RWA process. The electric field launched inside the cavity is shown in Figure 8(a). Figure 8(b) shows the electron beam moving along the cavity structure. One can observe in this figure that after acceleration the electrons go through the beam tunnel before striking the X-ray target. Most significantly, the electron beam energy as a function of distance is also shown in Figure 8(c). In this plot, one can clearly see that the electrons are gradually accelerated up to the target value of 200 keV before exiting the cavity.



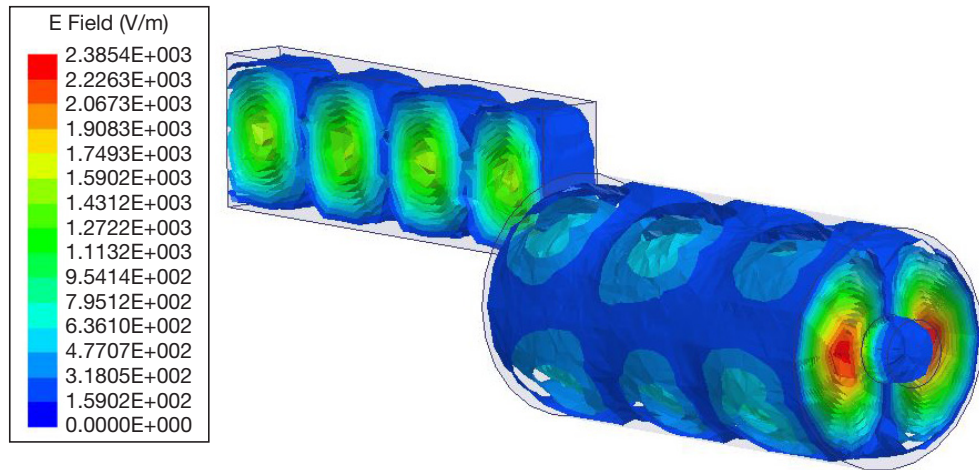


Figure 7. HFSS simulation result of the RWA cavity showing successful operation in the  $TM_{110}$  mode at 8 GHz.

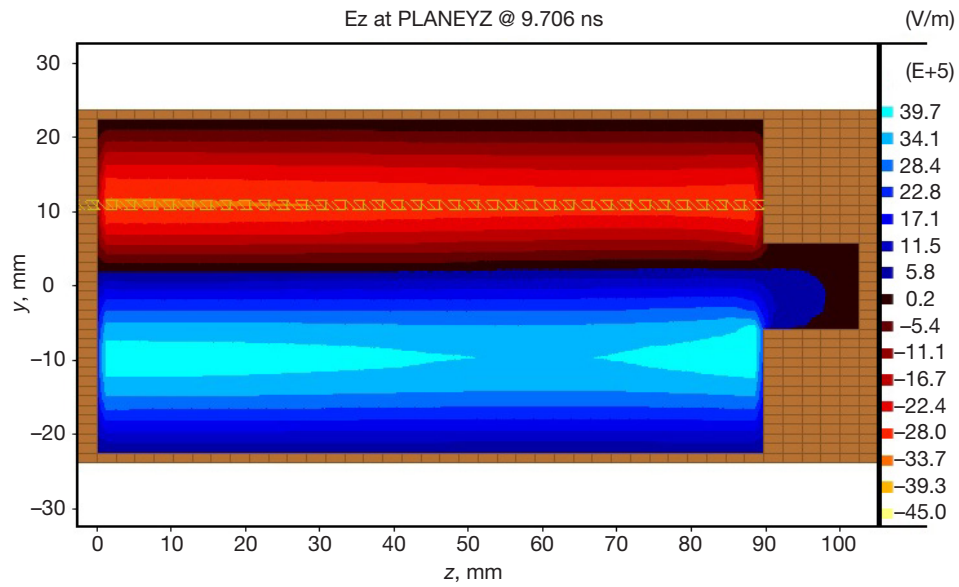


Figure 8(a). Typical MAGIC simulation results of the RWA. Shown here are the  $TM_{110}$  fields.

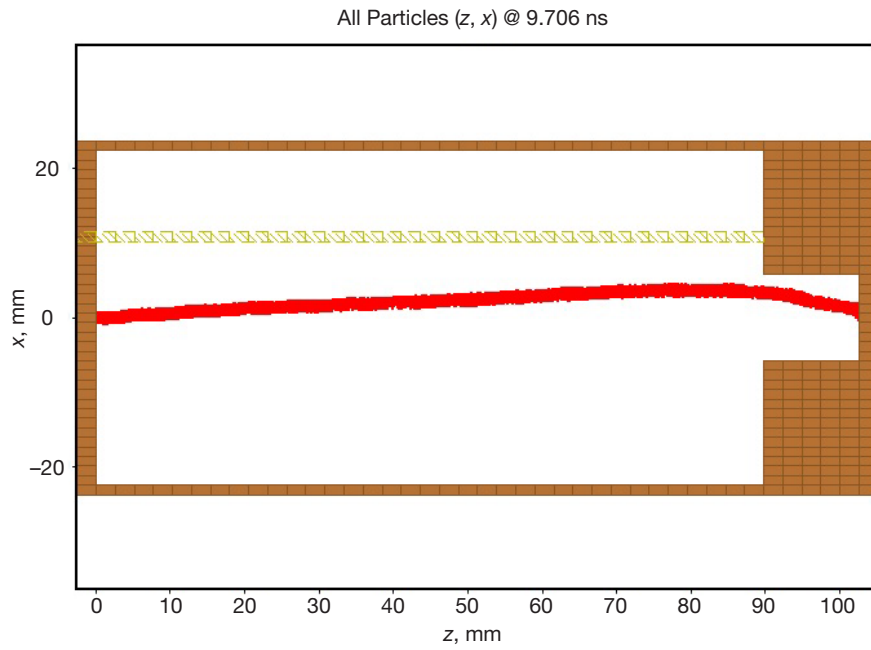


Figure 8(b). Typical MAGIC simulation results of the RWA. Shown here is the electron beam trajectory.

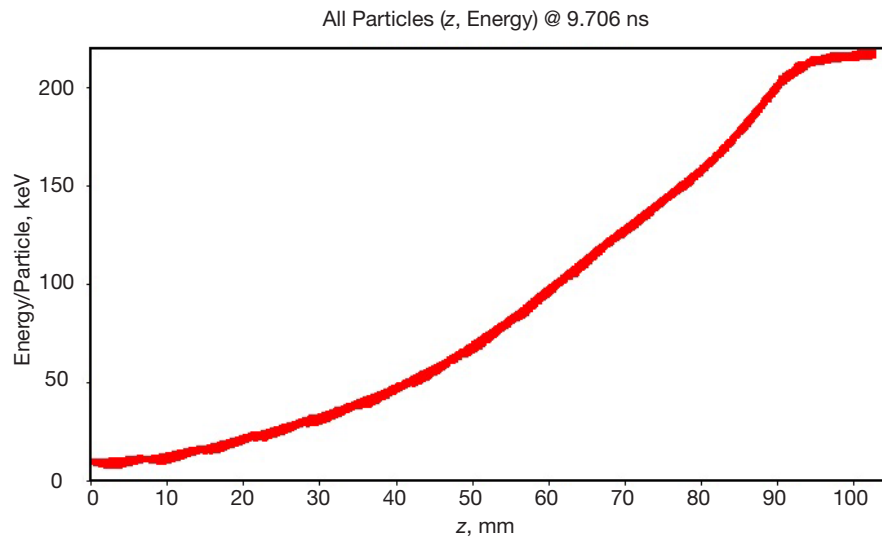


Figure 8(c). Typical MAGIC simulation results of the RWA. Shown here is electron energy as function of z.

## V. Conclusions

We have successfully demonstrated via sophisticated computer simulation studies that the RWXS is capable of producing high-energy X-rays. The RWXS will provide 200-keV X-rays while requiring operating voltages similar to or lower than 28 kV, which makes possible a new generation of scientific instruments for X-ray analysis of Martian and other planetary surfaces, and possibly orbital missions. The advantages of a high X-ray energy and high-flux source include X-ray analysis (e.g., fluorescence or tomography) with better depth penetration and the ability to excite the strong K lines of the entire periodic table. Such a source allows for standoff material composition analysis from several meters. An additional revolutionary feature is that the adjustable higher X-ray energies provided by this method are able to penetrate targets and provide information at various target depths using a combination of X-ray spectroscopy and backscatter imaging. To our knowledge, this feature is not provided by any other existing instrument deployed or planned to be deployed by NASA and will allow scientists to make measurements beyond the target's surface. Therefore, developing an RWXS will create a unique capability at JPL, which in turn increases JPL's potential in capturing funding for future planetary surface missions and instruments.

## References

- [1] R. Gellert, R. Rieder, J. Brückner, B. Clark, G. Dreibus, et al., "Alpha Particle X-Ray Spectrometer (APXS): Results from Gusev Crater and Calibration Report," *Journal of Geophysical Research: Planets*, vol. 111, issue E2, February 2006.  
<https://dx.doi.org/10.1029/2005JE002555>
- [2] D. Blake, D. Vaniman, C. Achilles, R. Anderson, D. Bish, et al., "Characterization and Calibration of the CheMin Mineralogical Instrument on Mars Science Laboratory," *Space Science Reviews*, September 2012, vol. 170, issue 1, pp. 431–399.  
<https://dx.doi.org/10.1007/s11214-012-9905-1>
- [3] A. Allwood, B. Clark, D. Flannery, J. Hurowitz, L. Wade, et al., "Texture-Specific Elemental Analysis of Rocks and Soils with PIXL: The Planetary Instrument for X-ray Lithochemistry on Mars 2020," *Proceedings of IEEE Aerospace Conference 2015*, March 7–14, 2015.  
<https://dx.doi.org/10.1109/AERO.2015.7119099>
- [4] J. E. Velazco and P. H. Ceperley, "Development of a Compact Rotating-Wave Electron Accelerator," *Proceedings of the 17th International Conference on the Application of Accelerators in Research and Industry (CAARI 2002)*, University of North Texas, Denton, Texas, PB9, p. 49, November 12–16, 2002.
- [5] P. H. Ceperley, J. E. Velazco, and D. M. Menz, "Compact Rotating-Wave Accelerator for Medical and Industrial Applications," *Bulletin of the American Physical Society*, 51, YP1 49, Quebec City, Quebec, Canada, October 23–27, 2000.
- [6] J. E. Velazco, "Study of Compact Rotating-Wave Accelerators for Medical and Industrial Applications," (Invited Paper), *Proceedings of the Fourteenth International Conference on the Applications of Accelerators In Research and Industry*, DE5, University of North Texas, Denton, Texas, November 6–9, 1996.  
<https://dx.doi.org/10.1063/1.52415>

- [7] J. Velazco, W. M. Black, T. Godlove, and F. Mako, "The Design of a Deflection Cavity for a New Microwave Amplifier," *Proceedings of IEEE Southeastcon Conference*, May 1990.
- [8] M. W. Black, J. E. Velazco, T. F. Godlove, and F. Mako, "Transverse-Modulation Klystron Design Considerations and Preliminary Results," *Proceedings of IEEE International Electron Devices Meeting*, December 8, 1991.
- [9] J. Velazco and F. Mako, "Limited Spatial Region for Beam-Wave Synchronous Interactions in Rotating Mode Resonators," *Applied Physics Letters*, vol. 63, p. 3087, 1993.  
<https://dx.doi.org/10.1063/1.110241>
- [10] J. Velazco and P. Ceperley, "A Discussion of Rotating Wave Fields for Microwave Applications," *IEEE Transactions on Microwave Theory and Techniques*, vol. 41, no. 2, February 1993.  
<https://dx.doi.org/10.1109/22.216476>
- [11] P. H. Ceperley and J. E. Velazco, "Tuning a Rotating Mode Resonator," *Review of Scientific Instruments*, vol. 66, no. 1, pp. 256–260, January 1995.  
<https://dx.doi.org/10.1063/1.1145268>
- [12] H. R. Jory and A. W. Trivelpiece, "Charged-Particle Motion in Large-Amplitude Electromagnetic Fields," *Journal of Applied Physics*, vol. 39, no. 7, p. 3053, June 1968.  
<https://dx.doi.org/10.1063/1.1656732>
- [13] J. E. Velazco, "Study of Rotating-Wave Electromagnetic Modes for Applications in Space Exploration," *The Interplanetary Network Progress Report*, vol. 42-206, Jet Propulsion Laboratory, Pasadena, California, pp. 1–16, August 15, 2016.  
[http://ipnpr.jpl.nasa.gov/progress\\_report/42-206/206A.pdf](http://ipnpr.jpl.nasa.gov/progress_report/42-206/206A.pdf)